

# A variable admittance control strategy for stable physical human–robot interaction

The International Journal of  
Robotics Research  
1–19  
© The Author(s) 2019  
Article reuse guidelines:  
sagepub.com/journals-permissions  
DOI: 10.1177/0278364919840415  
journals.sagepub.com/home/ijr  


Federica Ferraguti<sup>1</sup> , Chiara Talignani Landi<sup>1</sup>, Lorenzo Sabattini<sup>1</sup>,  
Marcello Bonfè<sup>2</sup>, Cesare Fantuzzi<sup>1</sup> and Cristian Secchi<sup>1</sup>

## Abstract

*Admittance control allows a desired dynamic behavior to be reproduced on a non-backdrivable manipulator and it has been widely used for interaction control and, in particular, for human–robot collaboration. Nevertheless, stability problems arise when the environment (e.g. the human) the robot is interacting with becomes too stiff. In this paper, we investigate the stability issues related to a change of stiffness of the human arm during the interaction with an admittance-controlled robot. We propose a novel method for detecting the rise of instability and a passivity-preserving strategy for restoring a stable behavior. The results of the paper are validated on two robotic setups and with 50 users performing two tasks that emulate industrial operations.*

## Keywords

physical human–robot interaction, cooperative manipulators, admittance control, human-in-the-loop

## 1. Introduction

In the last few years, the growing attention paid to physical human–robot interaction (pHRI) and collaborative robotics has allowed the old paradigm of robots working inside safety cages to be left behind, converting them into collaborators that work side by side with humans. Different tasks can be accomplished with robots, such as assisted industrial manipulation, collaborative assembly, domestic work, entertainment, rehabilitation, or medical applications. Owing to this tight cooperation and the coexistence of humans and robots sharing the same workspace, safety and dependability are of paramount importance.

Different approaches have been developed to implement a reliable pHRI, exploiting control strategies that make the robot compliant (see, e.g., Villani and De Schutter, 2008). In the industrial scenario, the admittance control is particularly appealing because it allows existing industrial, non-backdrivable, manipulators to be exploited. For example, admittance control has been used to implement robot manual guidance in Talignani Landi et al. (2016) and Ferraguti et al. (2017), by means of “walk-through programming” where the human operator becomes the teacher that physically guides the robot throughout the desired trajectory.

When using admittance-controlled robots, instability can arise when interacting with stiff environments. This can be due to several factors such as the robot structural dynamics, the limitations of the actuators, and the

implementations of low-level controllers (Eppinger and Seering, 1986). All these destabilizing effects are due to the violation of the co-location principle, as shown by Colgate and Hogan (1989).

As humans are dynamic systems characterized by a time-varying impedance, they can behave in a stiff way and, consequently, give rise to instability when interacting with admittance-controlled robots. Tsumugiwa et al. (2004) showed that this effect, combined with the time delay in the human reaction and the compliance in the robot structure, can cause instabilities during a cooperative transportation task. As shown by Peer and Buss (2008), instability is related to the human arm impedance, especially when the user grasps the tool placed on the end-effector in a very stiff way. Moreover, it is always possible to choose an admittance dynamics that makes the human–robot system unstable (Peer and Buss, 2008).

Instability induces, among other undesired effects, a deviation of the robot from the desired admittance

<sup>1</sup>Department of Science and Methods for Engineering, University of Modena and Reggio Emilia, Italy

<sup>2</sup>Engineering Department, University of Ferrara, Italy

## Corresponding author:

Federica Ferraguti, Department of Science and Methods for Engineering, University of Modena and Reggio Emilia, via Amendola 2, 42122 Reggio Emilia, Italy.

Email: federica.ferraguti@unimore.it

behavior. Furthermore, it produces high-amplitude oscillations of the end-effector, undermining the user safety during the interaction. Thus, it is very important to promptly detect the rise of oscillations and then act to restore a stable and safe behavior.

An effective method for recovering stability consists of modifying the admittance dynamics parameters. The most common strategy consists of increasing the desired damping of the admittance. This action increases the dissipation of the system and restores a passive and stable behavior. Nevertheless, a bigger damping factor affects the admittance dynamics and requires a larger effort for the human in the interaction with the robot (Dimeas and Aspragathos, 2016). Moreover, changing only one of the parameters completely unbalances the admittance dynamics, and this has a tremendous effect on the usability of the robot (Lecours et al., 2012).

In this paper we propose a novel methodology for detecting the rise of oscillations during the interaction between a human and an admittance-controlled robot and a passivity-based parametric adaptation of the admittance for restoring stable behavior. The proposed adaptation allows the adaptive dynamics to be kept similar to the nominal one in order to avoid unbalancing effects and to increase the usability of the system.

Preliminary results have been presented in Talignani Landi et al. (2017b) and Talignani Landi et al. (2017a). In this paper we present the following significant extensions.

- The heuristic for detecting instability proposed in Talignani Landi et al. (2017b) and Talignani Landi et al. (2017a) was based on an empirically chosen threshold. In this work, we propose a new methodology for automatically setting the detection threshold using a thorough statistical analysis.
- The passivity-based parametric adaptation proposed in Talignani Landi et al. (2017b) and Talignani Landi et al. (2017a) leads to a conservative approach because it treats all the degrees of freedom (DOFs) in the same way. In this paper, we overcome this limit adding a weighted energy allocation strategy in order to consider separately translations and rotations.
- We provide an extended experimental validation with a larger number of users and two robots (a Puma 260 and a KUKA LWR 4+) to demonstrate that the presented algorithm is hardware independent and user adaptive, without needing an initial profiling of the human operator. Moreover, we provide an experimental comparison with state-of-the-art methods that address the detection and handling of instability in admittance control.

The remainder of this paper is organized as follows. In Section 2, a comparison between our method and related work is presented. Section 3 gives background information on the admittance control and the main issues in human-robot interaction, whereas, in Section 4, the procedure to detect online the increasing oscillations is described.

Section 5 shows the methodology for parameter adaptation with weighted energy allocation. In Section 6, we describe the experiments carried out with two different robotic setups, where the objective was to perform a precision and a velocity task; subsequently, we show the results of the experimental comparison of the proposed method with state-of-the-art approaches. Finally, in Section 7, a discussion of the results is proposed and the conclusions are drawn.

## 2. Related work

Different approaches are available in the literature to overcome increasing instabilities during the pHRI in response to a high human arm stiffness. A first method consists of estimating the arm stiffness and adapting the controller parameters as a consequence. Tsumugiwa et al. (2002) proposed to increase the damping coefficient in proportion to the estimated stiffness of the human arm, in order to stabilize the system. However, the user physical effort was increased and a dynamic model of the arm was required. Duchaine and Gosselin (2008) first estimated the human arm stiffness with recursive experiments, then they found the Lyapunov function for the closed-loop system that allows the stability frontiers to be defined and the critical value of each impedance parameter. In particular, they fixed the mass to the value that makes the system critically stable, and they found the critical damping experimentally. In this case, the impedance parameters are fixed and cannot be changed during the task execution, and the stiffness estimation has to be done each time the user changes.

Another approach exploits electromyography (EMG) sensors to evaluate when the user is stiffening their arm. For example, in Gallagher et al. (2014), the information provided by the EMG sensor is used to estimate the muscle activity and, consequently, the user stiffness, adjusting the impedance controller parameters. In particular, the initial damping value is increased along with the user stiffness to counteract the oscillations and to allow the haptic device to be held steadily. The method of Grafakos et al. (2016) has a variable admittance control where the damping parameter is adjusted between two predefined values when the EMG sensors detect a co-contraction in the operator's arm muscles. In both cases only the damping increased, which requires larger human physical effort and additional sensors.

An example of an external device that helps in stabilizing the system was presented by Lamy et al. (2009): the designed handle, coated with foam that acts as a mechanical filter, is mounted on the robot end-effector and it is used to estimate the human grasping force during a co-manipulation task. The parameters in the designed PI robot controller are changed according to the performed estimation.

Other approaches, not requiring external devices or additional sensors, are based only on interaction force and end-

effector position measurements. For example, Erden and Marić (2011) presented a method that computes the variance of the measured tool positions during the performance phase of a welding task. This criterion takes into account the oscillations of the torch: the smaller the variance, the more successful the welding. Hence, a proper high damping value is determined, to obtain an effective vibration suppression during welding, whereas a low value is set during the movement of the torch from one point to another. They proved that this method helps untrained users, but they only switch between two damping values that are set a priori for all of the operators, excluding the possibility of tuning the parameters according to different users. Podobnik and Munih (2007) investigated the contact instability of the admittance control of a haptic interface. The human grasping force is measured and its critical value that destabilizes the system is determined. To improve stability two methods are applied: the first exploits the virtual coupling (i.e. an artificial link between the haptic display and a virtual environment); the second features a compensator used as a filter of the input force exerted by the human operator. Duchaine et al. (2012) proposed a method to estimate the interaction stiffness exploiting the force/torque sensor used for the admittance control. As a consequence, a stability observer is defined that detects oscillations and adapts the damping matrix in real time.

Approaches based on the frequency analysis of a signal (i.e. force, velocity, or position) are presented in Dimeas and Aspragathos (2016), Ryu et al. (2008), and Okunev et al. (2012). In Dimeas and Aspragathos (2016), a stability observer was proposed, based on the frequency analysis of the force signal generated from the interaction between the operator and the robot. Consequently, an instability index is built and the admittance parameters (i.e. inertia and damping) are increased proportionally. In Ryu et al. (2008), a haptic stability observer examines the motion in the frequency domain and quantifies the degree of instability. Hence, a damping force is generated by the controller to counteract the oscillations. A frequency analysis is done also in Okunev et al. (2012), where the fast Fourier transform (FFT) of the measured forces at the end-effector, in combination with boosted classifiers, allows instability oscillations to be detected and consequently the admittance control parameters to be modified. The performed simulations show that the primary method to avoid oscillations consists of increasing the inertia. Nevertheless, the frequency analysis introduces a delay in the compensation that can reduce its effectiveness.

The time-domain vibration observer presented by Campeau-Lecours et al. (2016) addresses the interaction stability issue by means of an adaptive control strategy. A vibration index is computed and then used to adjust the control gains in order to reduce the vibrations that appear when the operator grasps the end-effector in a stiff manner. Different control strategies are possible: the admittance control parameters (i.e. inertia and damping) can be linearly varied between two values, a damping can be added, or

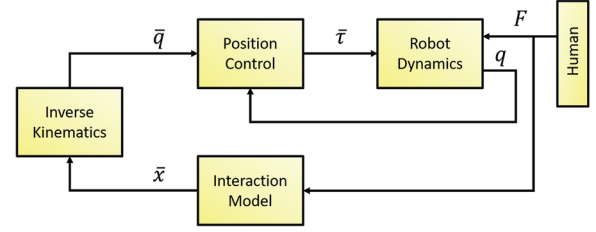


**Fig. 1.** Control scheme of the admittance control with underlying motion controller. The solution of the interaction model with the input  $F(t)$  provides the value  $\bar{x}$ , which the position-controlled robot must follow, by computing the desired joint positions  $\bar{q}$  from inverse kinematics and regulating the joint torque  $\tau$  to let the actual joint positions  $q$  track  $\bar{q}$ .

the low-level controller gains can be reduced. A common strategy, based on energy flow, that allows a haptic system to be controlled ensuring stable contact is the passivity observer (PO) and passivity controller (PC) implementation (Hannaford and Ryu, 2002). Nevertheless, as highlighted in Campeau-Lecours et al. (2016), the use of PO-PC during the interaction with a stiff user does not detect any instability oscillation. Indeed, in the PO output the energy does not become negative: the PC would apply corrections only when extra energy is injected into the system in response to an active behavior, but it would not apply any correction when the vibrations are due to a stiff but passive environment.

Unlike the presented approaches, our work aims at proposing a methodology for detecting the increasing oscillations in pHRI that is independent from the velocity and acceleration bounds of the robot and does not require external devices or frequency analysis computations. Furthermore, the proposed parameter adaptation strategy allows stability to be restored while preserving a passive behavior of the admittance dynamics. This is very important because changing parameters of a (virtual) physical dynamics can lead to a non-passive and, therefore, unstable dynamics. Thus, if passivity is not guaranteed, it may happen that the stabilizing mechanism (i.e. changing parameters) induces instability because of a loss of passivity.

### 3. Background on admittance control and issues in human–robot interaction

Consider an  $n$ -DOF manipulator controlled by using the admittance control scheme shown in Figure 1. Given a desired interaction model, namely a dynamic relation between the motion of the robot and the force applied by the environment, and given the external force, the admittance equation, via a suitable integration (see, e.g., De Stefano et al., 2017a,b for explicit passive integration strategies), generates the position and orientation to be used as a reference for a low-level position controller. The goal of the admittance control is to force the robot to behave

compliantly with the environment, according to a given mass–spring–damper system. The elastic part of this system is used to attract the robot end-effector towards a desired pose. However, because we want to address the case of a robotic manipulator manually driven by the human operator, in this paper we do not consider the elastic part of the general admittance control model (Villani and De Schutter, 2008). Indeed, the user guides the robot by means of the force applied to its end-effector, without directly specifying a desired pose. Let  $\bar{x}(t) \in \mathbb{R}^6$  be the set-point computed by the admittance controller and  $x(t) \in \mathbb{R}^6$  be the pose of the end-effector, obtained from the joint positions  $q(t) \in \mathbb{R}^m$ ,  $m \geq 6$ , through the forward kinematics. For ease of notation we hereafter omit the dependency of  $q(t)$  from  $t$ . We expect that the low-level position controller is designed and tuned to minimize the tracking error and optimize the dynamic response so that the robot can track a feasible set-point. Thus, we will make the following assumption.

**Assumption 1.** *The low-level position controller is designed and tuned in such a way that  $x(t) \simeq \bar{x}(t)$  as long as*

$$\begin{aligned} -\dot{\bar{x}}(q) &\leq \dot{x}(t) \leq \dot{\bar{x}}(q) \\ -\ddot{\bar{x}}(q) &\leq \ddot{x}(t) \leq \ddot{\bar{x}}(q) \end{aligned} \quad (1)$$

where

$$\begin{aligned} \dot{\bar{x}}(q) &= [\dot{\bar{x}}_1, \dots, \dot{\bar{x}}_6]^T \in \mathbb{R}^6 \\ \ddot{\bar{x}}(q) &= [\ddot{\bar{x}}_1, \dots, \ddot{\bar{x}}_6]^T \in \mathbb{R}^6 \end{aligned} \quad (2)$$

are configuration-dependent velocity and acceleration bounds due to the robot dynamics and the inequalities are component-wise.

We want to force the robot to interact with the environment according to the following desired behavior:

$$M_d \ddot{x}(t) + D_d \dot{x}(t) = F(t) \quad (3)$$

where  $M_d \in \mathbb{R}^{6 \times 6}$  and  $D_d \in \mathbb{R}^{6 \times 6}$  are the desired inertia and damping symmetric and positive-definite matrices. The external force  $F(t) \in \mathbb{R}^6$  in (3) is assumed to be measured by a 6-DOF force/torque (F/T) sensor attached at the robot wrist flange. The controlled robot behaves as (3) and it is passive with respect to the pair  $(F(t), \dot{x}(t))$ , as proved in Ferraguti et al. (2015).

During the execution of the cooperative task, the robot is coupled with a human operator, whose dynamics (e.g. change of compliance of the arm) can cause deviations from the desired behavior that may produce robot oscillating motions of high amplitude and frequency, making the interaction unsafe for the user (Dimeas and Aspragathos (2016)). Thus, the oscillations have to be detected and then the desired behavior has to be recovered.

A common strategy for restoring the desired behavior of the controlled robot in the presence of deviation is to adapt the parameters of the admittance control (Ranatunga et al.,

2017: see, e.g.,). As shown in Dimeas and Aspragathos (2016), three different adaptation laws can be used to stabilize the system: increase the damping, increase the inertia, or increase both the damping and the inertia while keeping a constant ratio. Thus, in order to be able to compensate the destabilizing effects by adapting the parameters, we implement the following, time-varying, interaction model:

$$M(t) \ddot{x}(t) + D(t) \dot{x}(t) = F(t) \quad (4)$$

where  $M(t) \in \mathbb{R}^{6 \times 6}$  and  $D(t) \in \mathbb{R}^{6 \times 6}$  are inertia and damping symmetric and positive-definite matrices such that  $M(0) = M_d$  and  $D(0) = D_d$ . While increasing the damping is an intuitive and passivity-preserving approach because it increases the energy dissipated, changing the inertia is, in general, a non-passive operation (Ferraguti et al., 2015). Thus, it may happen that the procedure for stabilizing the interaction makes the admittance dynamics non-passive and possibly unstable. Nevertheless, using the method explained in the following sections, it is possible to adapt both the damping and inertia parameters in (4) while preserving the passivity of the initial dynamics.

In Talignani Landi et al. (2017b), the following simple heuristic for detecting the rise of an oscillatory behavior during the cooperation has been proposed:

$$\|F(t) - M(t) \ddot{x}(t) - D(t) \dot{x}(t)\| \leq \varepsilon \quad (5)$$

where  $\varepsilon \in \mathbb{R}^+$  is an appropriately defined small threshold. When (5) is not satisfied, the robot is considered to be deviating from the interaction model imposed by the admittance control. Unfortunately, because oscillating motions have a high frequency, which corresponds to high values of velocities and accelerations, the threshold indicating such a deviation strongly depends on the maximum velocity and acceleration achievable by the robot and on the time-varying admittance parameters. This makes  $\varepsilon$  also time-varying and hard to tune. In Talignani Landi et al. (2017a), a novel condition for detecting the rise of high-frequency oscillations that is more robust than (5) has been proposed. However, the value of the detection threshold  $\varepsilon$  still has to be manually found through post-processing operations.

## 4. Online detection of increasing oscillations in pHRI

In order to overcome the drawbacks introduced by the use of real-time computations of (5) to detect the increasing oscillations, in this section we introduce an improved heuristic and a practical procedure for tuning the detection threshold  $\varepsilon$ .

### 4.1. Definition of the heuristic

Let us define the vectors  $\dot{\hat{x}}(t) \in \mathbb{R}^6$  and  $\ddot{\hat{x}}(t) \in \mathbb{R}^6$  as the tracking error derivatives scaled with respect to the bounds

$\dot{\mathcal{X}}$  and  $\ddot{\mathcal{X}}$ . In particular, the  $j$ th components of the scaled vectors are defined as follows:

$$\dot{\hat{x}}_j(t) = \frac{\dot{\hat{x}}_j(t)}{\dot{\hat{x}}_j(q)} \quad \ddot{\hat{x}}_j(t) = \frac{\ddot{\hat{x}}_j(t)}{\ddot{\hat{x}}_j(q)} \quad j = 1, \dots, 6 \quad (6)$$

where

$$\begin{aligned} \dot{\hat{\mathbf{x}}}(t) &= \dot{\hat{\mathbf{x}}}(t) - \dot{\mathbf{x}}(t) = [\dot{\hat{x}}_1(t) \dots \dot{\hat{x}}_6(t)]^T \in \mathbb{R}^6 \\ \ddot{\hat{\mathbf{x}}}(t) &= \ddot{\hat{\mathbf{x}}}(t) - \ddot{\mathbf{x}}(t) = [\ddot{\hat{x}}_1(t) \dots \ddot{\hat{x}}_6(t)]^T \in \mathbb{R}^6 \end{aligned} \quad (7)$$

are the first- and second-order derivatives of the tracking error. Robot velocities and accelerations can be measured using specific hardware (e.g. gyroscopes and accelerometers) or estimated using, for example, the quaternion-based Kalman filter introduced in Farsoni et al. (2017).

Moreover, we introduce the following damping-to-inertia ratio matrix:

$$R_d(t) = M^{-1}(t)D(t) \quad (8)$$

We can now define the improved heuristic in terms of (6) and (8), as follows:

$$\psi(\dot{\hat{\mathbf{x}}}(t), \ddot{\hat{\mathbf{x}}}(t)) = \|\ddot{\hat{\mathbf{x}}}(t) + R_d(t)\dot{\hat{\mathbf{x}}}(t)\| \leq \varepsilon \quad (9)$$

With a slight abuse of notation, we hereafter use  $\psi(t)$  to indicate the value of  $\psi(\dot{\hat{\mathbf{x}}}(t), \ddot{\hat{\mathbf{x}}}(t))$  at time  $t$ . We propose to use (9) as the heuristic for detecting online when oscillations occur. Namely, when (9) is not satisfied, we claim that oscillations are increasing. Unlike (5), this novel formulation of the detection index is intrinsically insensitive to the physical characteristics of the robot in use, thanks to the scaling with respect to velocity and acceleration bounds (6), and its sensitivity against the current values of inertia and damping matrices is mitigated. Indeed, (9) contains the damping-to-inertia ratio (8) that multiplies only the scaled velocity error, which is generally much smaller than the scaled acceleration error, in case of high-frequency oscillations.

#### 4.2. Experimental statistical characterization of the detection index $\psi(t)$

In the last part of this section (Section 4.3) we propose, as a novel contribution of this paper, a practical procedure to tune the detection threshold  $\varepsilon$ . The proposed procedure is based on the results of the following experimental characterization of the detection index  $\psi(t)$ . The characterization is based on statistical methods and on the following assumptions.

**Assumption 2.** *Given an initial choice of the admittance parameters  $M_d$  and  $D_d$  that is feasible for the characteristics of the robot (Lecours et al., 2012) and for the desired interaction task, an experienced human operator can interact properly with the robot (i.e. without causing oscillating*

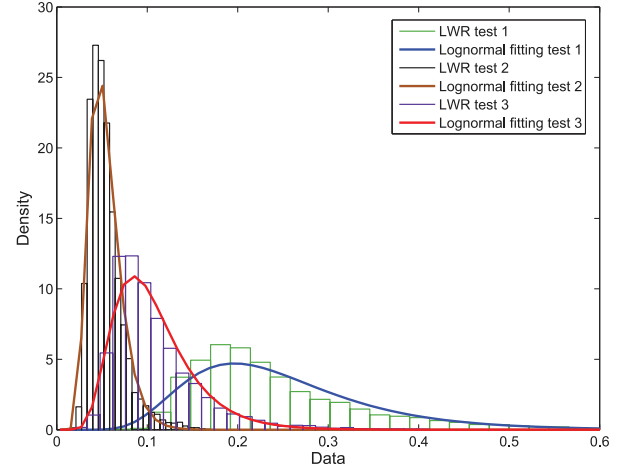


**Fig. 2.** Histogram distributions and fitted log-normal PDFs for the experiments with the KUKA LWR 4+ robot.

behaviors), applying a gentle grasp and softening their arm.

Assumption 2 is not restrictive in practice, provided that the chosen admittance parameters  $M_d$  and  $D_d$  are not excessively small (Lecours et al., 2012).

**Assumption 3.** *The detection index  $\psi(t)$  is a random variable whose probability density function (PDF), and its related cumulative distribution function (CDF), can be estimated from experimental data.*

Assumption 3 is derived from considering that the detection index  $\psi(t)$  is a function of the tracking error. As a robotic manipulator is a complex nonlinear system subject to different sources of uncertainty (e.g. measurement and modeling errors, external disturbances, etc.), its tracking error is generally described by means of non-Gaussian stochastic models (Chen et al., 2009).

**Assumption 4.** *The admittance control adaptation law (see Section 5.2) is designed to preserve a constant damping-to-inertia ratio.*

Assumption 4 represents a recommended practice in pHRI (see Lecours et al. (2012)). Indeed, this choice allows a similar dynamics of the system to be maintained after the adaptation, which is more intuitive for the operator rather than increasing only the inertia or only the damping. Assumption 4 implies that the threshold  $\varepsilon$  is tuned for a given initial value of the damping-to-inertia ratio  $R_d(0)$ , generally set according to the desired interaction task, and has to be re-tuned only if such a parameter setting is changed.

We performed several experiments in order to obtain the statistical characterization of the detection index  $\psi(t)$ . In particular, under Assumption 2, an experienced operator applied persistent inputs to  $F(t)$  and forced the robot to move within a large part of its workspace, while avoiding joint limits and singular configurations and without causing oscillations. Meanwhile, the value of  $\psi(t)$  is calculated and discrete-time samples are recorded. The time series of  $\psi(t)$



collected during the experiments were analyzed to search for a probability distribution properly fitting the data and thus to estimate the PDF and the related CDF.

In order to fully characterize the probability distribution of  $\psi(t)$ , the experiments were performed on two different robotic systems (a KUKA LWR 4+ and a Puma 260) with different (experienced) users who interacted with the admittance-controlled robots and with different values of the admittance model parameters. We chose diagonal inertia and damping matrices, resulting in diagonal damping to inertia ratio matrices. We performed the experiment with the following damping to inertia ratio on each robotic setup.

- *Test 1*: 12.5 kg Ns/m on translational DOFs and 25 kg Ns/mrad on rotational DOFs.
- *Test 2*: 1.25 kg Ns/m on translational DOFs and 2.5 kg Ns/mrad on rotational DOFs.
- *Test 3*: 5 kg Ns/m on translational DOFs and 10 kg Ns/mrad on rotational DOFs.

To define the PDF that best characterizes  $\psi(t)$ , we considered only distributions supported on the semi-infinite interval  $[0, \infty)$  (e.g. Birnbaum–Saunders, Gamma, log-logistic, log-normal, Weibull, etc.) (Johnson et al., 1995), being the values of  $\psi(t)$  strictly positive by definition. As a result of this study, the log-normal distribution was selected for the statistical characterization of the detection index  $\psi(t)$  because its goodness of fit was the best or the second best for all of the experiments and its parameters can be estimated with simple formulas, applying the maximum likelihood estimation (MLE) method (Ginos, 2009). The plots in Figures 2 and 3 show the histogram distributions of the data acquired during the three tests with, respectively, the KUKA LWR 4+ and the Puma 260, together with the log-normal PDFs whose parameters are calculated with MLE from such data. As can be seen, the two robotic systems provide similar experimental results, being the distributions centered on higher values of  $\psi(t)$  for higher damping-to-inertia ratios. Slight differences in the quantitative evaluations could be ascribed to the differences in the tracking performances of the low-level position controllers of the two robots.

As the different damping-to-inertia ratios result in similar robot behaviors, we chose the ratio of Test 1 and performed experiments under the following conditions:

- three different periods (30, 60, 120 seconds);
- three experienced users;
- two different values of inertia and damping (keeping the ratio constant according to Test 1).

In all of these cases, the estimated parameters of the log-normal distribution did not change significantly, leading to similar results in terms of PDF distribution fitting. The results of these experiments have shown that the log-normal is a good choice for characterizing the detection index  $\psi(t)$ .

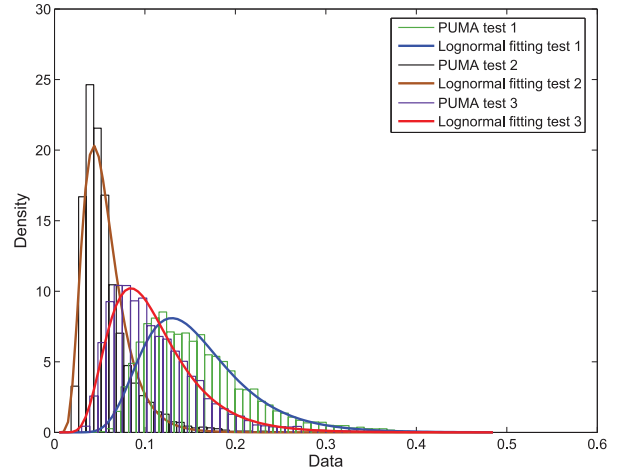


**Fig. 3.** Histogram distributions and fitted log-normal PDFs for the experiments with the Puma 260 robot.

This result will be used in the following section to define a procedure for the automatic tuning of the threshold  $\varepsilon$ .

#### 4.3. Procedure for tuning the detection threshold

According to the experimental results of Section 4.2 and to the characterization of the distribution of  $\psi(t)$  as a log-normal, we can define a procedure for tuning the detection threshold  $\varepsilon$  as follows.

1. Given initial values of inertia and damping matrices and, therefore, of the desired damping-to-inertia ratio matrix, the experienced operator applies persistent force stimuli to the admittance-controlled robot to move it in a wide portion of its workspace, while the control system logs the values of  $\psi(t)$  for at least 60 seconds.
2. The potential presence of a significant number of outliers in the recorded series of  $\psi(t)$  is detected. Indeed, outlying samples are potentially related to undesired oscillations that even the experienced user may have not perceived. As the log-normal is a *skewed* distribution, the outliers detection is based on the adjusted boxplot described by Hubert and Vandervieren (2008). Following this approach, a sample is considered to be an outlier if it falls outside of the interval:

$$[Q_1 - 1.5e^{-4MC}IQR, Q_3 + 1.5e^{3MC}IQR] \quad (10)$$

where  $Q_1$  and  $Q_3$  are the first and third quartile of the sampled data, respectively,  $IQR = Q_3 - Q_1$  is the interquartile range, and  $MC$  is the *medcouple*, a robust measure of skewness (Brys et al., 2004). Note that the proposed boxplot formula assumes  $MC > 0$ , since a log-normal distribution is *right* skewed. If the total number of outliers does not exceed 5% of the sampled data and consecutive outlying samples represent short time intervals (e.g. smaller than

200 ms), it can be concluded that experimental data do not include oscillating behaviors and can be used for the subsequent steps of the tuning procedure.

3. If outliers are negligible and the user acknowledges that the experimental run is valid for the tuning of the threshold, the PDF of  $\psi(t)$  is estimated from sampled data. In particular, the parameters of a log-normal distribution are estimated using the following MLE formulas (see Ginos (2009)):

$$\hat{\mu} = \frac{\sum_{i=0}^{N-1} \ln \psi(i \cdot T)}{N}; \quad \hat{\sigma} = \sqrt{\frac{\sum_{i=0}^{N-1} (\ln \psi(i \cdot T) - \hat{\mu})^2}{N}} \quad (11)$$

where  $T$  is the sampling period,  $N$  is the number of discrete-time samples of  $\psi(t)$  collected during the test, and  $\hat{\mu}$  and  $\hat{\sigma}$  are the estimated *location* and the estimated *scale* of the log-normal distribution (Johnson et al., 1995), respectively.

4. The threshold  $\varepsilon$  is fixed as the upper bound of the prediction interval calculated as the value at which the log-normal CDF reaches the confidence level  $\alpha = 0.9999$  (chosen with the aim to mostly avoid false-positive detections).

To validate the proposed method, we applied the described procedure on the data of the experiments reported in Figures 2 and 3. Table 1 shows the threshold  $\varepsilon$  that resulted from Tests 1, 2 and 3 being performed on each robotic setup by a specific user. Obviously, the value of the threshold changes depending on the damping to inertia ratio and on the robot being used. However, repeating each test with different (experienced) users and with different admittance parameters values (keeping a constant damping-to-inertia ratio) led to threshold values (not fully reported here for conciseness) changing only within a  $\pm 5\%$  interval with respect to those reported in Table 1. Therefore, we can conclude that, under Assumption 4, the threshold, automatically computed from a test run by an experienced user, can be used for online detection of increasing oscillations.

## 5. Methodology for parameter adaptation with weighted energy allocation

### 5.1. Passivity-based approach for restoring the desired behavior

In this section, we show how to adapt the parameters of the admittance control to restore the desired behavior of the controlled robot in the presence of high-frequency oscillations, identified according to the technique described in Section 4. If the parameters have to be adapted, then the desired interaction model becomes the variable admittance model (4). The main drawback due to the introduction of variable terms in an admittance control scheme is the loss of passivity of the controlled robot (see, e.g., Ferraguti

**Table 1.** Resulting detection threshold  $\varepsilon$  in different tests.

	Test 1	Test 2	Test 3
KUKA LWR 4 +	1.015	0.1698	0.4379
PUMA 260	0.5544	0.2410	0.4871

et al., 2015). This can be easily seen by considering the non-negative total energy as a storage function:

$$H(\dot{x}(t)) = \frac{1}{2} \dot{x}(t)^T M(t) \dot{x}(t) \quad (12)$$

The variation of the energy function is given by

$$\dot{H}(\dot{x}(t)) = \dot{x}(t)^T M(t) \ddot{x}(t) + \frac{1}{2} \dot{x}(t)^T \dot{M}(t) \dot{x}(t) \quad (13)$$

Using (4) in (13) we obtain

$$\dot{H}(\dot{x}(t)) = \dot{x}(t)^T F(t) + \frac{1}{2} \dot{x}(t)^T (\dot{M}(t) - 2D(t)) \dot{x}(t) \quad (14)$$

Owing to the variability of the inertia matrix, the term between brackets can be positive and, therefore, some extra energy can be injected into the system by the controller. This effect would destroy passivity and lead to a potentially unstable and unsafe behavior of the robot.

In order to guarantee the passivity, we exploit the concept of energy tanks that allows the use of the (virtual) energy circulating in the controlled system in a flexible and passivity-preserving way (see, e.g., Ferraguti et al., 2015; Franken et al., 2011; Secchi et al., 2006)). Indeed, the energy dissipated by the system is stored in a virtual energy reservoir, the *tank*, and can be reused for implementing any desired control action in a passivity-preserving way. For this purpose, we augment the dynamics (4) as follows:

$$\begin{cases} M(t)\ddot{x}(t) + D(t)\dot{x}(t) = F(t) \\ \dot{z}(t) = \frac{\varphi(t)}{z(t)} P_D(t) - \frac{\gamma(t)}{z(t)} P_M(t) \end{cases} \quad (15)$$

where

$$P_D(t) = \dot{x}(t)^T D(t) \dot{x}(t) \quad P_M(t) = \frac{1}{2} \dot{x}(t)^T \dot{M}(t) \dot{x}(t) \quad (16)$$

are the dissipated power due to the damping, and the dissipated/injected power due to the inertia variation, respectively, and  $z(t) \in \mathbb{R}$  is the state of the tank. Furthermore, let

$$T(z(t)) = \frac{1}{2} z(t)^2 \quad (17)$$

be the energy stored in the tank. We hereafter assume that  $\exists \delta, \bar{T}$ , with  $0 < \delta < \bar{T}$ , such that  $\delta \leq T(z(t)) \leq \bar{T}$ , for all  $t$ . The upper bound is guaranteed by the parameters  $\varphi(t) \in \{0, 1\}$  and  $\gamma(t) \in \{0, 1\}$  that disable the energy storage in case a maximum, application-dependent, limit  $\bar{T} \in \mathbb{R}^+$  is reached. It is necessary to bound the available

energy because, if there were no bounds, the energy could become very high as time increases and, even if the system keeps on being passive, it would be possible to implement practically unstable behaviors (Lee and Huang, 2010)). In particular,

$$\varphi(t) = \begin{cases} 1 & \text{if } T(z(t)) \leq \bar{T} \\ 0 & \text{otherwise} \end{cases} \quad (18)$$

enables/disables the storage of dissipated energy, while

$$\gamma(t) = \begin{cases} \varphi & \text{if } \dot{M}(t) \leq 0 \\ 1 & \text{otherwise} \end{cases} \quad (19)$$

enables/disables the injection ( $\dot{M}(t) \leq 0$ ) of energy into the tank due to the inertia variation but it always allows ( $\dot{M}(t) > 0$ ) energy to be extracted from the tank. The lower bound, required for avoiding singularities in (15), is guaranteed by carefully planning/forbidding the extraction of energy when  $T(z(t)) = \delta$  is reached. Note that the extraction of energy is due only to  $P_M(t)$ . The tank initial state is set to  $z(0)$  such that  $T(z(0)) > \delta$ .

The evolution of the energy in the tank can be written as

$$\dot{T}(z(t)) = z(t)\dot{z}(t) = \varphi(t)P_D(t) - \gamma(t)P_M(t) \quad (20)$$

Using the augmented dynamics it is possible to prove the following result.

**Proposition 1.** *If  $T(z(t)) \geq \delta$  for all  $t \geq 0$ , the system (15) is passive with respect to the pair  $(F(t), \dot{x}(t))$ .*

*Proof.* Consider the following positive storage function:

$$W(\dot{x}(t), z(t)) = H(\dot{x}(t)) + T(z(t)) \quad (21)$$

where  $H(\dot{x}(t))$  is defined in (12) and  $T(z(t))$  in (17). With a slight abuse of notation we will hereafter use  $W(t)$ ,  $H(t)$ , and  $T(t)$  to indicate the value of  $W(\dot{x}(t), z(t))$ ,  $H(\dot{x}(t))$ , and  $T(z(t))$  at time  $t$ , respectively. We have that

$$\begin{aligned} \dot{W}(t) &= \dot{H}(t) + \dot{T}(t) = \dot{x}(t)^T F(t) - (1 - \varphi(t))P_D(t) \\ &\quad + (1 - \gamma(t))P_M(t) \end{aligned} \quad (22)$$

As  $\varphi(t) \in \{0, 1\}$  and  $P_D(t) \geq 0$ , we have that

$$\dot{x}(t)^T F(t) \geq \dot{H}(t) + \dot{T}(t) - (1 - \gamma(t))P_M(t) \quad (23)$$

If  $\dot{M}(t) \leq 0$ , then, from (16) and from (19), it follows that  $-(1 - \gamma(t))P_M(t) \leq 0$ . In case  $\dot{M}(t) > 0$ , from (19), it follows that  $\gamma(t) = 1$  and, consequently,  $(1 - \gamma(t))P_M(t) = 0$ . Thus, from (22) we can obtain

$$\dot{x}(t)^T F(t) \geq \dot{H}(t) + \dot{T}(t) \quad (24)$$

which implies

$$\begin{aligned} \int_0^t \dot{x}(\tau)^T F(\tau) d\tau &\geq H(t) - H(0) + T(t) - T(0) \\ &\geq -H(0) - T(0) \end{aligned} \quad (25)$$

which proves passivity.  $\square$

Thus, as long as there is energy available in the tank, it is possible to implement any kind of inertia variation. Nevertheless, it is important to guarantee that the variation of the inertia does not deplete the tank. Indeed, if this happens, all the active behaviors (e.g. increasing of inertia) would be stopped and this would lead to unwanted behaviors (e.g. oscillations) in the cooperative system. In the following, we propose a condition on the variation of the inertia that guarantees that the tank never depletes and, as a consequence, that the system remains passive.

We assume that the inertia variations take place in pre-defined finite intervals (e.g. when the user stiffens their arm). As clearly shown in (15) and in (16), energy can be extracted by the tank only if  $\dot{M}(t) > 0$ . Thus, it is necessary to bound the increase of inertia depending on the energy stored in the tank. Consider a generic time interval  $[a, b]$  where  $\dot{M}(t) > 0$ . From (19),  $\gamma(t) = 1$  for all  $t \in [a, b]$ . From (20), the energy of the tank at  $t = b$  is given by

$$\begin{aligned} T(b) &= T(a) + \int_a^b P_D(\tau) d\tau - \int_a^b P_M(\tau) d\tau \geq T(a) \\ &\quad - \int_a^b P_M(\tau) d\tau \end{aligned} \quad (26)$$

In order to avoid depleting the tank during the variation interval, because  $\dot{M}(t) > 0$  for all  $t \in [a, b]$ , it is sufficient that  $T(b) \geq \delta$ , namely, using (26):

$$T(a) - \int_a^b P_M(\tau) d\tau \geq \delta \quad (27)$$

which can be reformulated as

$$\int_a^b P_M(\tau) d\tau \leq T(a) - \delta \quad (28)$$

namely that the energy extracted in the interval is at most equal to the energy initially available beyond the lower bound  $\delta$ .

As the desired inertia and damping are parameters that can be freely chosen, provided that they are symmetric and positive-definite matrices, we consider the following assumption.

**Assumption 5.** *The desired inertia and damping in (4) are diagonal matrices and they are defined as*

$$\begin{aligned} M(t) &= \text{diag}\{m_1(t), \dots, m_6(t)\} \\ D(t) &= \text{diag}\{d_1(t), \dots, d_6(t)\} \end{aligned} \quad (29)$$

As  $M(t)$  is diagonal,  $\dot{M}(t)$  is also diagonal and its eigenvalues are the elements on the diagonal.

With this assumption, we can decouple the different components (e.g. the translational components from the rotational ones). Indeed, the following inequality holds:



**Algorithm 1:** Parameter Adaptation

---

**Data:**  $M(0), D(0), \beta, \varepsilon, \Delta t, \Delta M, \mathcal{A}$

- 1 initialize  $k = 0, \zeta_0 = 0, \zeta = \{\zeta_0\}, S_0 = 0_6$
- 2 compute damping to inertia ratio:  $R_d(0) = M^{-1}(0)D(0)$
- 3 **for**  $i = 0$  **to**  $\infty$  **do**
- 4   compute the detection index  $\psi(t_i) = \|\ddot{\mathbf{x}}(t_i) + R_d(0)\dot{\mathbf{x}}(t_i)\|$
- 5   **if**  $\psi(t_i) > \varepsilon$  **then**
- 6      $k = k + 1$
- 7     update vector of oscillations occurrences  $\zeta_k = t_i$
- 8     **for**  $j = 1$  **to**  $6$  **do**
- 9       compute amount of inertia variation
- 10        $s_j = \min\left\{\frac{2\alpha_j(T(t_i) - \delta)}{\bar{\mathcal{X}}_j^2}, \bar{m}_j\right\}$
- 11     **end**
- 12      $S_i = \text{diag}\{s_1, \dots, s_6\}$
- 13   **end**
- 14   update inertia  $M(t_{i+1}) = M(0) + \sum_{p=0}^k S_p \beta^{(t_{i+1} - (\zeta_p + \Delta t))}$
- 15   update damping  $D(t_{i+1}) = R_d(0)M(t_{i+1})$
- 16 **end**

---

$$\int_a^b P_M(\tau) d\tau \leq \sum_{j=1}^6 \frac{1}{2} \bar{m}_j \bar{\mathcal{X}}_j^2 (b - a) \quad (30)$$

where  $\bar{m}_j$  ( $j = 1, \dots, 6$ ) are bounds on  $\dot{m}_j(t)$  for all  $t \in [a, b]$  and  $\bar{\mathcal{X}}_j = \max_q \dot{\mathcal{X}}_j(q)$  ( $j = 1, \dots, 6$ ) are component-wise upper bounds on the robot velocity limits defined in Assumption 1. On the other hand, if we define a vector of weights  $\mathcal{A} = \{\alpha_1, \dots, \alpha_6\}$ , such that

$$\sum_{j=1}^6 \alpha_j = 1 \quad (31)$$

and we use these weights to distribute the energy available in the tank at the beginning of the adaptation period on the 6 DOFs of robot motion

$$T(a) - \delta = \sum_{j=1}^6 \alpha_j (T(a) - \delta) \quad (32)$$

then it is possible to write the following inequalities:

$$\frac{1}{2} \bar{m}_j \bar{\mathcal{X}}_j^2 (b - a) \leq \alpha_j (T(a) - \delta) \quad \forall j = 1, \dots, 6 \quad (33)$$

Consequently, the condition on the inertia variations that allows passivity to be preserved, with a weighted distribution of the energy extracted from the tank within the adaptation interval, can be stated as follows:

$$\dot{m}_j(t) \leq \bar{m}_j \leq \frac{2\alpha_j (T(a) - \delta)}{\bar{\mathcal{X}}_j^2 (b - a)} \quad \forall j = 1, \dots, 6 \quad (34)$$

This newer formulation of the passivity-preserving adaptation law, with respect to that used in Talignani Landi et al. (2017a,b), allows us to take into account that the velocity bounds of the robot may be quite different on the different

DOFs, especially comparing translational and rotational ones. Thanks to the component-wise definition of the inertia variation bound and to a proper choice of the weights vector  $\mathcal{A}$ , the adaptation of the admittance parameters related to each DOF can be tuned more precisely, according to the features of the robot and to the desired task. Intuitively, lower weights should be specified for the components related to rotational DOFs, whose corresponding elements on the diagonal of  $M(t)$  tends to be smaller than those related to translational DOFs (i.e. the values in the inertia tensor of a rigid body are, in general, quantitatively smaller than its mass). On the other hand, the oscillating behavior of the human-robot interaction can be counteracted with smaller inertia variations on those DOFs for which higher velocities are admissible. More details on the tuning of the weights vector are given in Section 6.

## 5.2. Algorithm for parameter adaptation in admittance control

Section 5.1 provided a possible way for using (34) to adapt the parameters of the admittance control to recover a stable behavior of the human-robot interaction when oscillations are detected. In the following, we provide a procedure for parameter adaptation, that allows the parameters to increase only when required due to the detection of increasing oscillations, but then restores the desired interaction model when such oscillations disappear (e.g. due to a relaxation of the operator's arm). The parameters will be adapted according to the component-wise passivity-preserving bound defined by (34). The algorithm will be provided in the discrete-time domain in order to be implementable on a real robotic system. The conditions on the time derivatives stated so far can be approximated using the corresponding difference quotient for a sufficiently small sampling period. We will then consider a set of time intervals  $[t_i, t_{i+1}]$ , with  $i = 1, 2, \dots$  and such that  $t_{i+1} - t_i = \Delta t$ , within which the parameter adaptation takes place. In particular, Algorithm 1 shows how the admittance parameters are updated.

Once increasing oscillations have been detected, the algorithm allows us to compute the variation of the inertia that satisfies the passivity constraints and the stability of the system is recovered. The variation of the damping is performed according to a constant damping-to-inertia ratio ( $R_d(t) = R_d(0), \forall t \geq 0$ ). Thus, the first step of the algorithm is the computation of the damping-to-inertia ratio according to (8) and based on the desired inertia matrix  $M(0)$  and damping matrix  $D(0)$  (line 2). Then, at each time instant  $t_i$ , the detection index defined in (9) is computed (line 4). If oscillations are increasing, (9) is not satisfied and the oscillatory behavior is detected in line 5, where  $\varepsilon > 0$  is a threshold previously defined using the procedure proposed in Section 4. The vector  $\zeta$  stores all the instants in which oscillations are detected. Thus, at line 7 a new element  $\zeta_k$  is inserted in  $\zeta$  and it is associated to the current instant of time  $t_i$  which corresponds to the instant of detection. In this

case, the admittance parameters have to be adapted for restoring the stability of the system. In particular, under condition (33) and Assumption 5, integrating (34), we obtain that each component of the inertia matrix can be passively increased as follows

$$m_j(t_{i+1}) - m_j(t_i) = \frac{2\alpha_j(T(t_i) - \delta)}{\dot{\chi}_j^2} \quad \forall j = 1, \dots, 6 \quad (35)$$

It is worth noting that (35) represents the maximum allowed inertia variation, based on the energy contained in the tank at time  $t = t_i$ . In practical cases, this value can be very large: thus, direct application of (35) would lead to an excessively large inertia variation. For this reason, we define an upper-bound  $\Delta M = \text{diag}\{\bar{m}_1, \dots, \bar{m}_6\}$  on the allowed inertia variation as follows:

$$m_j(t_{i+1}) - m_j(t_i) \leq \bar{m}_j \quad \forall j = 1, \dots, 6 \quad (36)$$

Under such a condition, the amount of variation of the inertia can be computed component-wise as the minimum between the allowed inertia variation (35) and the upper-bound (36) (line 9):

$$s_j = \min \left\{ \frac{2\alpha_j(T(t_i) - \delta)}{\dot{\chi}_j^2}, \bar{m}_j \right\} \quad \forall j = 1, \dots, 6 \quad (37)$$

The empirical definition of the bounds  $\bar{m}_j$  is a practical necessity and has been exploited in the experiments described in Talignani Landi et al. (2017a,b) also to take into account that some DOFs (i.e. generally rotational ones) may require smaller values of inertia variations. However, the newer definition of the inertia adaptation law, based on the weighted distribution of the tank energy, allows the inertia variations to be modulated more precisely thanks to the choice of the weights vector and the component-wise scaling by the velocity bounds  $\dot{\chi}_j$ . Indeed, in the experiments reported in Section 6, the conservative bounds  $\bar{m}_j$  were rarely enforced.

The single components computed in (37) are then used in Line 11 to fill the matrix of inertia variation as follows:

$$S_i = \text{diag}\{s_1, \dots, s_6\} \quad \forall i = 1, 2, \dots \quad (38)$$

The final part of the algorithm is the actual variation of the admittance parameters. The inertia variation is computed in line 13 as follows:

$$M(t_{i+1}) = M(0) + \sum_{p=0}^k S_p \beta^{(t_{i+1} - (\tau_p + \Delta t))} \quad (39)$$

where  $\beta$  ( $0 < \beta \leq 1$ ) is a forgetting factor that allows the desired interaction model (3) to be gradually restored. Indeed, the presence of the forgetting factor  $\beta$  in the second term in the right-hand side of (39) makes the effect of each inertia increase negligible after a certain amount of time. In particular, this time is larger for higher values of  $\beta$ . Note

that the inertia increases only at each time instant when a deviation is detected, as a consequence of (39). In all the other instants, the inertia only decreases and this has been shown in Talignani Landi et al. (2017b) to be a passivity-preserving operation.

Finally, the damping is updated preserving the constant damping-to-inertia ratio as follows:

$$D(t_{i+1}) = R_d(0)M(t_{i+1}) \quad (40)$$

## 6. Experiments

The proposed adaptation strategy has been validated by means of experiments performed on two different robotic systems and involving a total of 50 users (13 female, 37 male, from 22 to 44 years old), divided into four groups: two of 12, one of 15, and one of 18 users. Since industrial tasks typically require a combination of precision and execution speed, we implemented two tasks focused on the two separate aspects. Each group of users was asked to interact with one of the robots to perform one of the tasks. Therefore, the four groups experienced two different tasks on two different robots, with a minimal overlap of people in the four experiences. The two robotic setups consisted of:

- a Puma 260 6-DOF robot with a retrofitted control hardware, embedding six Gold Solo Whistle servo drives from Elmo Motion Control, and a wrist-mounted six-axis F/T sensor, made by the IIT research institute;
- a KUKA LWR 4+ 7-DOF robot, equipped with a ATI Mini 45 six-axis F/T sensor and configured in its (non-compliant) joint position control mode.

The control software has been implemented using the Orocos Real-Time Toolkit (RTT) and Kinematics/Dynamics Library (KDL)<sup>2</sup> and is the same on the two robots, excluding only hardware interface components (i.e. using the Fast Research Interface on the KUKA robot and the EtherCAT fieldbus on the Puma 260). Even the sampling times of the admittance controller and of the parameter adaptation algorithm, respectively set to 2 and 4.5 ms, are the same on the two systems.

Velocity and acceleration limits of the two robots are imposed, at joint level, by the servo drives on the Puma 260 and by a bank of nonlinear filters (Gerelli and Bianco, 2009) smoothing the joint position commands on the KUKA LWR 4+. In this way, such limits can be arbitrarily configured on both systems, while the joint position control mode of the KUKA LWR 4+ would not provide this feature. Cartesian velocity and acceleration limits (i.e.  $\dot{\chi}(q)$  and  $\ddot{\chi}(q)$ ) are then computed online via the Jacobian and Jacobian derivative matrices depending on the current joints configuration. In this way the detection index  $\psi(t)$  is precisely computed according to (9) on the basis of the dynamic bounds corresponding to the current robot pose. A constant upper bound for the velocity limits (i.e.  $\dot{\chi}$ ) to

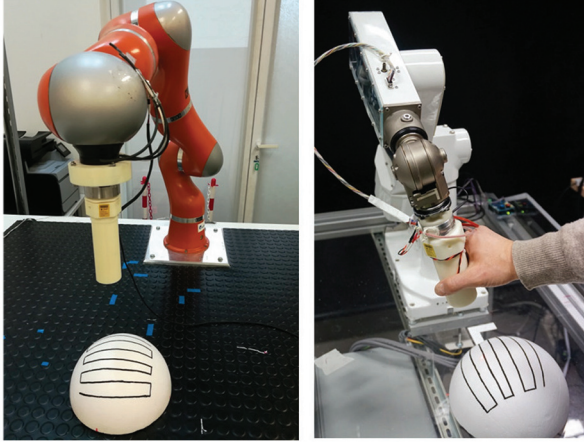


**Fig. 4.** Setup of the laser-tracking task on the KUKA LWR 4+ (left) and on the Puma 260 (right).

be used for the admittance control adaptation law (35), was then defined after experimental observations performed in the reduced part of the workspace interested by the two tasks. In particular, the velocity bounds to be used in (35) are fixed as  $\dot{\mathcal{X}} = \{2.50, 2.50, 2.50, 24, 24, 24\}$  for the Puma 260 and  $\dot{\mathcal{X}} = \{2.30, 2.30, 2.30, 6, 6, 6\}$  for the KUKA LWR 4+. The vectors of weights, whose components are used in (35) to distribute the energy available in the tank during the adaptation, are set to  $\mathcal{A} = \{0.25, 0.25, 0.25, 0.1, 0.1, 0.05\}$  for the Puma 260 and  $\mathcal{A} = \{0.3, 0.3, 0.3, 0.04, 0.04, 0.02\}$  for the KUKA LWR 4+. This choice of the velocity bounds and of the weights vectors in (35) allows similar adaptive behaviors to be achieved on the two robots.

According to the theory developed in Sections 3 and 5, some design choices were made. In particular, the energy thresholds, required by the passivity-preserving mechanism of Section 5, have been selected as  $\delta = 0.1 J$  and  $\bar{T} = 5 J$ . The initial value for the state of the tank is set to  $z(0) = 2$ , so that the initial energy contained in the tank, computed according to (17) results in  $T(0) = 2 J > \delta$ .

The objective of the proposed experiments is to validate usability and portability across different robotic systems of the proposed adaptive admittance control method, even in absence of an accurate and, possibly, task-dependent or robot-dependent tuning of the admittance parameters. For this reason, we used the same initial values of admittance control parameters on both robots and for both interaction tasks. In particular, such values of the inertia and damping matrices were set as

$$M(0) = \text{diag}\{M_1, M_2\} \quad D(0) = \text{diag}\{D_1, D_2\} \quad (41)$$

with

$$\begin{aligned} M_1 &= \text{diag}\{1, 1, 1\} \text{ kg} & M_2 &= \text{diag}\{0.1, 0.1, 0.1\} \text{ kg/m}^2 \\ D_1 &= \text{diag}\{4, 4, 4\} \text{ Ns/m} & D_2 &= \text{diag}\{0.4, 0.4, 0.4\} \text{ Nms/rad} \end{aligned}$$

Finally, the same values were used on both robots for the time interval of the adaptation, set to  $\Delta t = 4.5 \text{ ms}$ , the forgetting factor, chosen as  $\beta = 0.98$ , and the upper bounds on inertia variation, i.e.

$$\Delta M = \text{diag}\{0.5, 0.5, 0.5, 0.005, 0.005, 0.005\}$$

In the following, we present the two tasks that emulate industrial applications involving manual guidance of the manipulators, and the results collected during the interaction of the 50 users with the robots. Moreover, the users were asked to fill in the questionnaire proposed in Schmidler et al. (2017) in order to obtain a qualitative evaluation of the human–robot interaction from the user’s perspective. The two tasks have been implemented on both robotic setups. Some representative runs of the performed experiments are shown in the video in Extension 1.

### 6.1. Precision task: tracking a line on a spherical surface

In the first task, the users were asked to manually drive the end-effector of the robot, equipped with a handle embedding a laser pointer. The goal was to track, with the light dot, a path drawn on the surface of a sphere. This kind of task emulates industrial applications where the robotic tool has to precisely follow a contour (e.g. welding). All the DOFs of the manipulator are involved. Figure 4 shows the setup of the two robotic systems for the laser-tracking task.

More precisely, the task involves the following steps.

- The user grabs the handle, which is initially far from the spherical target, and brings it as fast as possible towards the drawn path.
- When the handle is at 10 cm from the sphere, the laser pointer is switched on automatically and a timer measuring the task completion time is started.
- The user has to lead the light dot through the drawn path, from a given initial point to a given ending point and back, as quickly as possible and keeping the light dot as close as possible to the path.

The data collected during the experiment are used to extract a quantitative evaluation of the task execution, in terms of: task completion time; number of zero-crossings in the Cartesian velocities of the robot end-effector (i.e. quantifying the smoothness of the task execution); root mean square (RMS) of the tracking error, measured as the distance from the projection of the light dot on the sphere to the closest point on the path; RMS of the F/T vector measured by the F/T sensor on the handle.

A group of 12 users interacted with the KUKA LWR 4+ and a group of 18 users interacted with the Puma 260. In both cases, each user performed the task three times, with a different setting of the adaptation strategy, as follows.

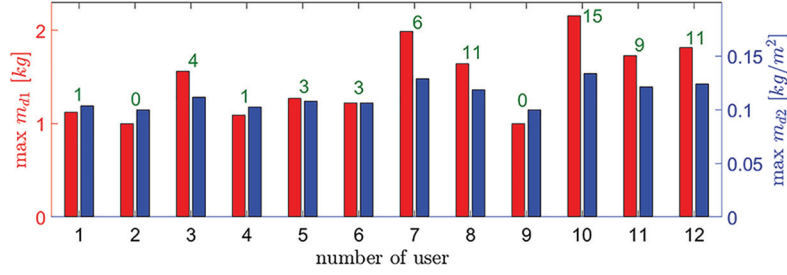


**Fig. 5.** Laser-tracking task on KUKA LWR 4+: maximum values of the inertia reached through the parameter adaptation, on translational DOFs (red columns) and rotational DOFs (blue columns). The number of detections triggering the adaptation is reported on top of the columns.

- **Control Mode 1.** The adaptation mechanism is triggered according to the detection threshold properly tuned with the procedure defined in Section 4, that resulted as  $\varepsilon = 0.16$  on the Puma robot and  $\varepsilon = 0.2$  on the KUKA robot. The damping-to-inertia ratio is computed from the parameters (41).
- **Control Mode 2.** The adaptation mechanism is triggered according to a detection threshold either underestimated (on the KUKA setup, i.e. modifying  $\varepsilon = 0.1$ ) or over-estimated (on the Puma setup, i.e. modifying  $\varepsilon = 0.32$ ), to evaluate the effects of, respectively, an unnecessarily frequent or an untimely adaptation. The damping-to-inertia ratio is the same as in the previous control mode.
- **Control Mode 3.** The adaptation mechanism is disabled and the admittance controller has the following constant parameters, much higher than the initial values of the adaptive model:

$$M_d = \text{diag}\{M_{d1}, M_{d2}\} \quad D_d = \text{diag}\{D_{d1}, D_{d2}\}$$

with

$$\begin{aligned} M_{d1} &= \text{diag}\{8, 8, 8\} \text{ kg} & M_{d2} &= \text{diag}\{0.25, 0.25, 0.25\} \text{ kg/m}^2 \\ D_{d1} &= \text{diag}\{32, 32, 32\} \text{ Ns/m} & D_{d2} &= \text{diag}\{1.0, 1.0, 1.0\} \\ && & \text{Nms/rad} \end{aligned}$$

As users were not allowed to test the system before the three experiments, the control modes were applied in a random order for each user, to avoid numerical results being affected more by the self-training induced by previous execution of the task, rather than by the control mode itself.

The first result that we could observe is related to the influence of the detection threshold on the adaptive admittance control behavior. Indeed, experiments on the KUKA robot with an under-estimated threshold revealed a mean number of adaptations per user of 16.75 (maximum 31, user #9), while in the experiments with the properly tuned threshold the mean was 5.33 (maximum 15, user #10). Conversely, the mean number of adaptations on the Puma robot with an over-estimated threshold was 1.22 (maximum

9, user #18), smaller than the mean of 2.94 (maximum 11, user #4) of the experiments with the properly tuned threshold. It should also be remarked that the number of adaptations is not as large as could be expected, considering that the initial values of the admittance parameters are set purposefully low and, therefore, prone to generating oscillations. However, the laser-tracking task induced the users to focus more on the tracking performance, rather than focusing on the completion time, and this behavior led them to apply soft and smooth inputs to the handle. As a consequence, the maximum values on the inertia matrix did not change much with respect to the initial setting. Figure 5 shows the maximum inertia values reached during the task being performed on the KUKA robot. Similar results were obtained on the Puma setup.

Another interesting aspect of the adaptation results is the fact that the inertia increasing mechanism was most frequently triggered at the beginning of the experiment, when the user had to grab the handle and to bring the robot near to the sphere. Indeed, during this phase users were more focused on the rapidity of motion and, therefore, they grabbed the handle more firmly and applied sharper forces. As an example, Figure 6 shows the evolution over time of the inertia along the  $x$ -direction for the experiment being performed by user #7 on the Puma 260.

The quantitative results collected during the task execution have been evaluated applying a two-way analysis of variance (ANOVA), with the aim of comparing the effect of control mode and user-specific capabilities as the two factors influencing the observations. Table 2 lists the  $p$ -values

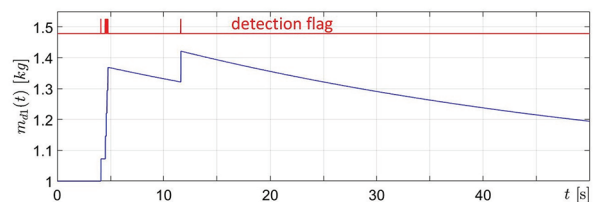


**Fig. 6.** Evolution over time of the inertia on a translational DOF for one user performing the laser-tracking task, with properly tuned detection threshold, on the Puma 260 setup.

**Table 2.** Results of two-way ANOVA on user tests for the laser-tracking task.  $p$ -values lower than 0.05 (highlighted cells) suggests that there is a relevant effect due to the related factor.

Setup		Time		Zero crossings		Force RMS		Tracking error RMS	
		Mode	Users	Mode	Users	Mode	Users	Mode	Users
<b>PUMA</b>	$p$ -value	0.499	0	0.511	0	0.006	0	0.511	0.609
<b>KUKA</b>	$p$ -value	0.203	0	0.345	<0.001	0	0.097	0.297	0.2565

that resulted for the laser-tracking task. A  $p$ -value lower than a given significance level (generally 0.05) suggests that there is a relevant effect due to the related factor. The results show that the only quantity that is significantly influenced by the control mode is the RMS value of the force input, while most of the other quantities are only influenced by the capabilities of the user. In other words, there were faster and slower users, but both fast and slow users obtained very similar performances with each control mode. Instead, no significant differences on the tracking errors are found. On the other hand, the number of velocity zero-crossings is not significantly affected by the control mode, revealing that the adaptation mechanism allows increasing oscillations to be promptly inhibited, so that human-robot interactions are as smooth as those governed by fixed high values of admittance control inertia and damping. The high values of the parameters imposed in control mode 3, however, play an important role on the physical effort required by the human, measured by the force RMS. The increased effort is clearly evident in Figure 7, where the three control modes are compared in terms of RMS of the force applied by the user during the task execution. Indeed, control modes 1 and 2 required a reduced effort to the user, since the adaptation algorithm allows us to set low initial inertia and damping parameters that are automatically adapted if oscillations arise.

Finally, a subjective qualitative evaluation has been obtained asking users to complete the Questionnaire for Physical Assistive Devices (QUEAD) proposed by Schmidtler et al. (2017), including a total of 16 statements, to be scored with a number from 1 (entirely disagree) to 7 (entirely agree), and related to five aspects of human-robot interaction: usefulness, ease of use, emotions, attitude, and comfort. Users were instructed to refer their evaluation to the adaptive control mode with the properly tuned detection threshold (control mode 1), but also to give their order of preference for the three control modes tested. Table 3 shows that the mean values of the qualitative evaluation are high (always higher than 4.75 out of maximum level of 7) on all the features. Moreover, the order of preference was evaluated by giving 3 points to the preferred control mode, 2 points to the second best, and 1 point to the last preferred. Summing the results of the 30 users testing either the Puma or the KUKA, the adaptive control mode with properly tuned threshold obtained 66 points, the non-adaptive control mode 63, and the adaptive control mode

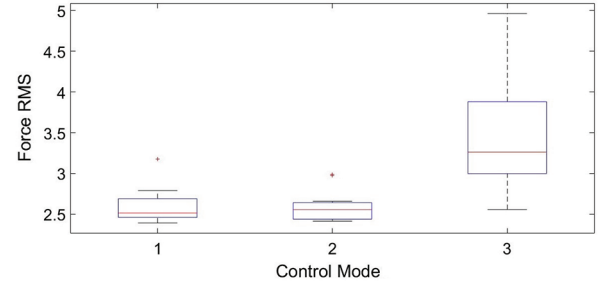


**Fig. 7.** Boxplots that compare the RMS of the force applied by the user to drive the robot during the laser-tracking task on the KUKA setup and with the three control modes.

with under-estimated or over-estimated threshold 51. It is important to remark that these results are actually affected by the choice of the initial parameters of inertia and damping. Indeed, high admittance parameters have been chosen when the users tested the non-adaptive control mode, in order to avoid frequent instabilities and oscillations. If lower parameters were chosen, users could have better appreciated the advantages of the adaptive control mode, but it may have been more difficult for them to complete the task, due to frequent instabilities. Moreover, it can be noted that the adaptive control mode with under-estimated or over-estimated threshold is rated lower than the non-adaptive control mode. This result is not surprising, since the detection threshold is a critical parameter in the proposed method. If the threshold is not tuned correctly, the results of the adaptation can be even worse with respect to the standard admittance control with high parameters. From this, one can assess the importance of an automatic tuning procedure of the detection threshold, such as that proposed in Section 4.3, eliminating the chance for incorrect threshold estimation.

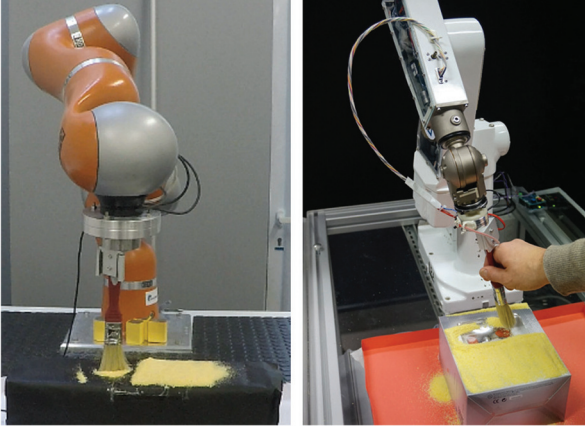
## 6.2. Rapidity task: brushing off a flat surface

In the second task, a soft brush has been mounted on the end-effector of the robots, as shown in Figure 8, and users were asked to clean colored dust from a flat surface, applying motions mimicking a painting task. In this case, precise movements are not required and the task completion time becomes the most significant quantitative aspect. As the role of the detection threshold has already been shown by



**Table 3.** Results of qualitative evaluations of the laser-tracking task with QUEAD (Schmidtler et al., 2017).

Setup	Usefulness	Ease of use	Emotions	Attitude	Comfort
<b>PUMA</b>	4.75	5.15	5.03	5.05	4.94
<b>KUKA</b>	5.33	5.6	5.51	5.5	6.11

**Fig. 8.** Setup of the brushing task on the KUKA LWR 4+ (left) and on the Puma 260 (right).

the results of the laser-tracking task, the brushing task has been executed by the users only with the properly tuned adaptive control mode (control mode 1) and with the non-adaptive mode (control mode 3).

Users were instructed to execute the operation as fast as possible. This objective induced the users to grab the brush firmly and apply high and sharp forces, leading to high levels of increasing oscillations in the human–robot interactive behavior. As a result, the parameter adaptation strategy was triggered much more frequently compared with the laser-tracking task. Figure 9 shows the inertia values of the 12 users that performed the task with the KUKA robot. Similar results were obtained on the Puma setup.

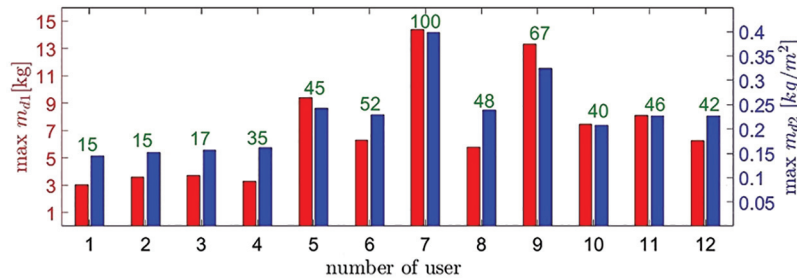
The results of the two-way ANOVA, reported in Table 4, are related to the same quantities recorded for the laser-tracking task, excluding the tracking error RMS. The table

shows that the control mode has a strong influence on the number of zero-crossings for the experiments performed on the Puma robot, but not for the experiments performed on the KUKA setup. In our opinion, this result is motivated by the fact that the Puma robot has a smaller workspace than the KUKA's one and thus the users had to work on a smaller surface and were induced to perform shorter motion cycles, repeated several times. This behavior resulted in purposefully oscillating behaviors in control mode 1 (small initial inertia and damping) that produced a higher number of velocity zero-crossings, even though not all of these oscillations triggered the parameter adaptation. On the KUKA setup, instead, users had to clean a bigger surface and they generally applied motions cycles with a larger range, but repeated less frequently. This behavior can also be related to a stronger grasp on the brush and a higher RMS value of the applied force, both with the adaptive control mode and with the non-adaptive one. Indeed, the ANOVA result about the effect of control mode on force RMS is not significant.

The results of the qualitative evaluation with the QUEAD, reported in Table 5, are slightly higher than those collected for the tracking task. Moreover, when asked to indicate their preferred control mode, 21 of the 27 total users selected the adaptive admittance control, which is a more definite preference compared with that expressed on the laser-tracking task.

### 6.3. Adaptation strategy assessment and comparison

In order to demonstrate the effectiveness of the overall detection and adaptation strategy, we performed experiments to show how the heuristic introduced in Section 4 detects the oscillatory behavior of the robots and the way

**Fig. 9.** Brushing task on KUKA LWR 4+ : maximum values of the inertia reached through the parameter adaptation, on translational DOFs (red columns) and rotational DOFs (blue columns). The number of detections triggering the adaptation is reported on top of the columns.

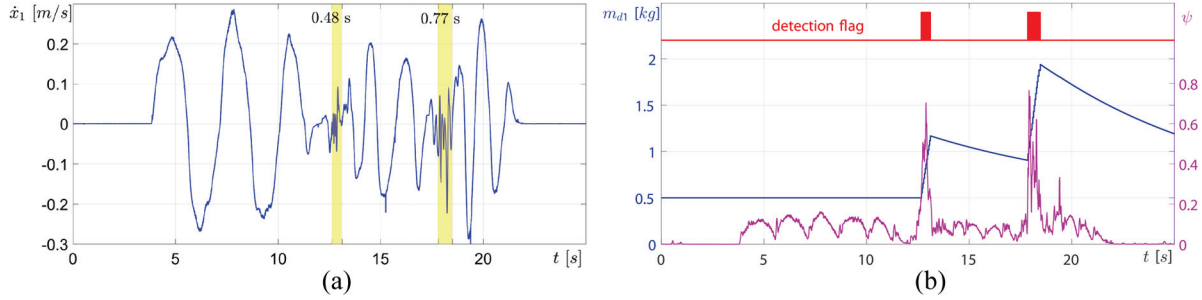


**Table 4.** Results of two-way ANOVA on user tests for the brushing task.  $p$ -values lower than 0.05 (highlighted cells) suggests that there is a relevant effect due to the related factor.

Setup		Time		Zero-crossings		Force RMS	
		Mode	Users	Mode	Users	Mode	Users
PUMA	$p$ -value	0.091	<b>0.001</b>	<b>&lt; 0.001</b>	<b>0.002</b>	<b>&lt; 0.001</b>	<b>&lt; 0.001</b>
KUKA	$p$ -value	<b>0.009</b>	<b>0.043</b>	0.232	0.314	<b>0.361</b>	<b>&lt; 0.001</b>

**Table 5.** Results of qualitative evaluations of the brushing task with QUEAD (Schmidtler et al., 2017).

Setup	Usefulness	Ease of use	Emotions	Attitude	Comfort
PUMA	5.33	5.73	5.68	6.1	5.7
KUKA	5.5	5.85	5.61	5.83	6

**Fig. 10.** Detection and adaptation of the increasing oscillations using the proposed method. (a) Velocity of the robot along the considered translational DOF. (b) Evolution over time of the detection index  $\psi(t)$  (magenta line), and of the subsequent inertia adaptation (blue line). A detection flag (red line) is added to show when the heuristic detects that oscillations are increasing.

stability is restored thanks to the adaptation strategy presented in Section 5. Moreover, experiments to compare the proposed approach with state-of-the-art methods are presented. In particular, we considered the methods proposed in Campeau-Lecours et al. (2016) and Dimeas and Aspragathos (2016).

First, specific experiments have been performed in order to test the heuristic and how the adaptation is used to handle the oscillatory behavior. These specific experiments have been performed restricting robot motion to only one translational DOF, in order to obtain results that can be fairly compared with those presented in the mentioned references. The inertia and damping initial parameters have been set equal to  $m(0) = 0.5$  kg and  $d(0) = 5$  kg/m<sup>2</sup>, because these values have been found by Dimeas and Aspragathos (2016) to be the minimum stable admittance gains for a KUKA LWR 4+, which is also the robot used in our experiments. Under these conditions, the detection threshold has been properly tuned with the procedure defined in Section 4.3 and the result was  $\varepsilon = 0.22$ . Whenever the user excessively stiffens their arm, high-frequency oscillations appear in the velocity of the robot

(Figure 10(a)). Figure 10(b) shows, in magenta, the evolution over time of the detection index  $\psi(t)$  as defined in (9). A Boolean detection flag is depicted with a red line in Figure 10(b). As can be seen, the increasing oscillations are correctly detected and the inertia (blue line) is adapted accordingly. As shown in Figure 10(a), when an oscillating behavior arises (yellow regions), the adaptation of the parameters allows the system to be stabilized 0.48 s after the occurrence of the first oscillation and 0.68 s after the occurrence of the second oscillation. Obviously, the difference in the adaptation times is due to the different attitude of the operator during the interaction, the different amplitude of the oscillations and, finally, to the starting values of the parameters when the adaptation is performed. However, thanks to the user study provided in Sections 6.1 and 6.2, we could verify that, from the user perspective, all the adaptation periods were sufficiently short amounts of time, since the adaptation of the parameters was achieved before the user could actually feel the increasing oscillations.

Then, we performed similar experiments applying our implementation of the methods proposed in Campeau-Lecours et al. (2016) and Dimeas and Aspragathos (2016).

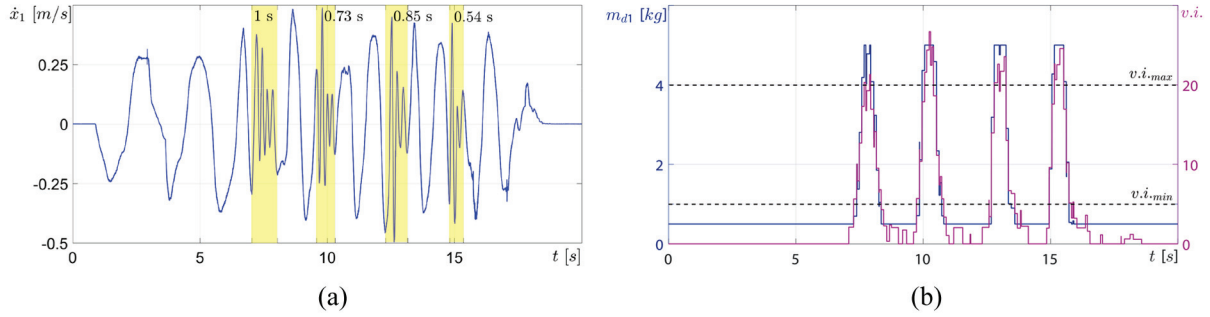


**Fig. 11.** Detection and adaptation of the increasing oscillations using the method proposed by Campeau-Lecours et al. (2016). (a) Velocity of the robot along the considered translational DOF. (b) Evolution over time of the variation index (magenta line) and of the inertia variation (blue line).

The results of the comparison are analyzed in the remainder of this section. As stated previously, the experiments consider only one translational DOF and initial inertia and damping parameters are set equal to  $m(0) = 0.5$  kg and  $d(0) = 5$  kg/m<sup>2</sup> for all the compared methods. Moreover, the same experienced user performed all the interaction tests for this comparison, aiming to minimize the inherent variability on the conditions of the experiment due to human behavior. An alternative solution to avoid such a variability could be the use of a variable stiffness apparatus emulating the average stiffness levels of a human arm, as suggested by Dimeas and Aspragathos (2016). Figure 11 shows the results of the implementation of the approach presented in Campeau-Lecours et al. (2016), based on the real-time computation of a vibration index, from minima and maxima detected on the robot velocity estimation, and the adaptation of admittance parameters by changing inertia and damping according to the vibration index. More precisely, if the vibration index is lower than a threshold  $v.i._{min}$ , the admittance parameters are set to their initial values  $m(0)$  and  $d(0)$ ; if the index exceeds an upper bound  $v.i._{max}$ , they are set to higher values, expected to guarantee a stable interaction (in our experiments,  $10 \cdot m(0)$  and  $10 \cdot d(0)$ ), and the parameters are changed from lower to higher values according to a linear function of the vibration index, during transient conditions. It is also important to remark that Campeau-Lecours et al. (2016) suggested the use of the vibration index to adapt also the gains of the inner robot motion controller, which is not feasible in our setup. In particular, Figure 11(a) shows the velocity of the robot and the regions where oscillations arise (yellow regions), while Figure 11(b) shows the evolution over time of the variation index (red line) and of the inertia variation (blue line).

Campeau-Lecours et al. (2016) provided guidelines to render the approach robust against the noise of the signal (i.e. by tuning a parameter called the narrow time window). However, in practical implementations, a significant level of noise may require additional countermeasures to reduce its impact. Indeed, as shown in Figure 12, without additional signal filtering and a threshold-based logic to discard

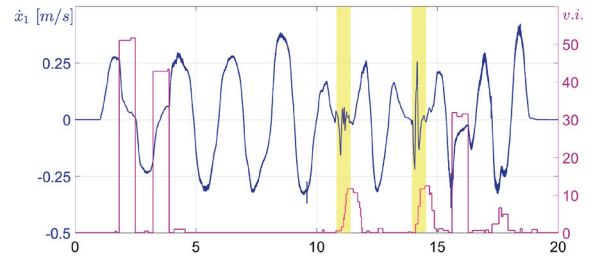


**Fig. 12.** Evolution over time of the velocity of the robot (blue line) and of the variation index (red line) in case that no additional filtering or threshold-based noise mitigation solutions are included in the method proposed by Campeau-Lecours et al. (2016).

minima and maxima due to noise, the index becomes quite large even in absence of oscillations (e.g. in the time intervals [7.8, 8.5] s and [9.2, 9.9] s). In these cases the index would be misleading in detecting the increasing oscillations. Moreover, the method proposed by Campeau-Lecours et al. (2016) requires the tuning of two different time windows and two thresholds, to be performed empirically. In the method presented in the current paper the detection threshold is automatically found by applying the procedure described in Section 4.3 and the detection index is not affected by noise, provided that a very simple debouncing logic is applied to avoid false positives. Figure 13 shows the results of the implementation of the approach presented by Dimeas and Aspragathos (2016), suggesting a peculiar formulation of a frequency-based instability index, which is then directly summed to the initial values of the admittance parameters. In particular, Figure 13(a) shows the velocity of the robot and the regions where oscillations arise (yellow regions), whereas Figure 13(b) shows the evolution over time of the inertia variation, that is given by the sum of the instability index and the initial inertia (0.5 kg).

The method presented in Dimeas and Aspragathos (2016) is not explicitly presented for the multi-DOF case. Indeed, the frequency-based instability index requires the calculation of the FFT on a moving time window, which

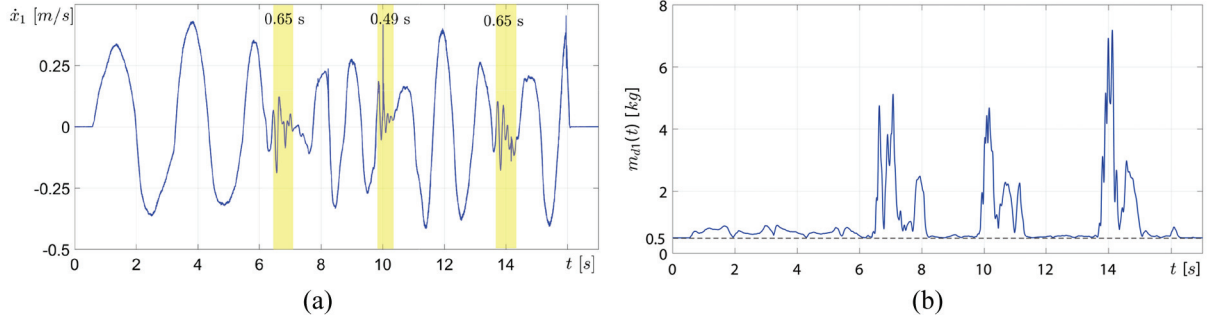


**Fig. 13.** Detection and adaptation of the increasing oscillations using the method proposed by Dimeas and Aspragathos (2016). (a) Velocity of the robot along the considered translational DOF. (b) Evolution over time of the inertia variation, given by the sum of the instability index and the initial inertia (0.5 kg).

**Table 6.** Time required for computing the detection index ( $\mu$ s).

Method	Mean value	Standard deviation	Min	Max
<b>Proposed in this paper</b>	17.46	0.46	16.81	59.62
<b>Proposed in Campeau-Lecours et al. (2016)</b>	458.03	10.25	426.76	571.37
<b>Proposed in Dimeas and Aspragathos (2016)</b>	206.39	6.30	197.02	273.40

can be computationally onerous if applied on multiple DOFs. Table 6 presents a comparison between the times required for computing the detection index during the experiments performed applying the three methods (i.e. that proposed in this paper, that presented by Campeau-Lecours et al. (2016), and that presented by Dimeas and Aspragathos (2016)). The detection index proposed in this paper requires only the instantaneous computation of the norm defined in (9), whereas both of the other approaches require time windows of several hundreds of samples to be processed. Moreover, the analysis is performed on the implementation for only one DOF. The time required by our proposed method is already calculated considering the multi-DOF case.

On the other hand, an interesting aspect of the methods proposed by Campeau-Lecours et al. (2016) and Dimeas and Aspragathos (2016) is the fact that the admittance parameters are explicitly calculated according to the detection index, considering that high values of inertia and damping related to high values of the detection index inherently lead to a reduction in such a vibration/oscillation index. This relationship could also be taken into account, together with the passivity-preserving variation of the inertia, in the method proposed here.

## 7. Discussion and conclusion

Admittance control is a widely used approach for guaranteeing a compliant behavior of the robot in pHRI. When an admittance-controlled robot is coupled with a human operator, the dynamics of the human can cause deviations from

the desired behavior, that is the one imposed by the admittance control. The deviations result in high-amplitude oscillations of the robot end-effector that may render the interaction with the robot unsafe for the user.

In this paper, we have presented a strategy for detecting the increasing oscillations and adapting the parameters of the admittance control to restore the stability. To detect the increasing oscillations, a heuristic has been defined. A procedure for automatically tuning the detection threshold used in the heuristic has been proposed, by exploiting statistical methods. We then provided an algorithm for adapting the parameters of the admittance control when it is necessary, i.e. when a increasing oscillation is detected, while preserving the passivity of the system. The parameters are gradually restored when the destabilizing factors are no longer active. An extensive validation has been performed on two robotic setups, with several users that performed two different tasks. The analysis of quantitative and qualitative results obtained during the experiments revealed that the proposed admittance adaptation strategy is capable of addressing the issue of increasing oscillations in human-robot interactions with a minimal robot-dependent tuning, limited to those parameters strictly affected by the dynamic bounds of the robot. Other settings of the adaptation strategy are instead quite independent of the features of the robot. With regard to the dependency on the task, instead, it should be remarked that initial values of the inertia and damping matrices could be tuned according to the requirements of the task itself and, possibly, according to a user-specific selection. For example, allowing a user to practice the human-robot interaction for a longer time, with the only purpose of training the walk-through

functionality for a given task, would probably allow us to establish the admittance control parameter settings more comfortably for that user (i.e. less prone to generate increasing oscillations because of the stiffness of their arm and their grasp on the robot end-effector). The forgetting factor for restoring the initial interaction model after an inertia augmentation is another parameter that could be user- and/or task-dependent.


However, these aspects were not investigated in this paper, whose objective is to present the passivity-preserving inertia adaptation strategy and a novel method for tuning of the oscillation detection threshold.

These issues remain an open problem. Together with the consideration of safety-related problems in industrial applications, solving these issues would lead to move a significant step towards implementation of the proposed strategy in a real industrial setup. Along these lines, the system can be rendered compliant with the international norms for collaborative robots (ISO 10218-1:2011, ISO 10218-2:2011, ISO/TS 15066:2016, see Rosenstrauch and Kruger (2017)). Moreover, the proposed methodology can be integrated with other solutions as, e.g., those that render the admittance parameters explicitly dependent from the detection index.

## Funding

This research received no specific grant from any funding agency in the public, commercial, or not-for-profit sectors.

## ORCID iD

Federica Ferraguti  <https://orcid.org/0000-0002-4989-1567>

## Notes

1. The choice of diagonal matrices is aimed at simplifying the notation for the comparison. Indeed, the desired inertia and damping matrices can be freely chosen, provided that they are symmetric and positive definite.
2. See <http://www.orocos.org>

## References

- Brys G, Hubert M and Struyf A (2004) A robust measure of skewness. *Journal of Computational and Graphical Statistics* 13(4): 996–1017.
- Campeau-Lecours A, Otis M, Belzile P and Gosselin C (2016) A time-domain vibration observer and controller for physical human–robot interaction. *Mechatronics* 36: 45–53.
- Chen H, He G, Xing J, Wang H and Chen L (2009) PDF control of tracking error of robotic systems with any bounded stochastic disturbances. In: *Proceedings of the 4th IEEE Conference on Industrial Electronics and Applications*, pp. 1636–1641.
- Colgate E and Hogan N (1989) The interaction of robots with passive environments: application to force feedback control. In: *Advanced Robotics*. Berlin: Springer-Verlag.
- De Stefano M, Artigas J and Secchi C (2017a) A passive integration strategy for rendering rotational rigid-body dynamics on a robotic simulator. In: *Proceedings of the IEEE/RSJ International Conference on Intelligent Robots and Systems*, pp. 2806–2812.
- De Stefano M, Balachandran R, Artigas J and Secchi C (2017b) Reproducing physical dynamics with hardware-in-the-loop simulators: A passive and explicit discrete integrator. In: *Proceedings of the IEEE International Conference on Robotics and Automation*, pp. 5899–5906.
- Dimeas F and Aspragathos N (2016) Online stability in human–robot cooperation with admittance control. *IEEE Transactions on Haptics* 9(2): 267–278.
- Duchaine V and Gosselin C (2008) Investigation of human–robot interaction stability using Lyapunov theory. In: *Proceedings of the IEEE International Conference on Robotics and Automation*, pp. 2189–2194.
- Duchaine V, St-Onge BM, Gao D and Gosselin C (2012) Stable and intuitive control of an intelligent assist device. *IEEE Transactions on Haptics* 5(2): 148–159.
- Eppinger S and Seering W (1986) On dynamic models of robot force control. In: *Proceedings of the IEEE International Conference on Robotics and Automation*.
- Erden MS and Marić B (2011) Assisting manual welding with robot. *Robotics and Computer-Integrated Manufacturing* 27(4): 818–828.
- Farsoni S, Talignani Landi C, Ferraguti F, Secchi C and Bonfè M (2017) Compensation of load dynamics for admittance controlled interactive industrial robots using a quaternion-based Kalman filter. *IEEE Robotics and Automation Letters* 2(2): 672–679.
- Ferraguti F, Preda N, Manurung A, et al. (2015) An energy tank-based interactive control architecture for autonomous and tele-operated robotic surgery. *IEEE Transactions on Robotics* 31(5): 1073–1088.
- Ferraguti F, Talignani Landi C, Secchi C, Fantuzzi C, Nolli M and Pesamosca M (2017) Walk-through programming for industrial applications. *Procedia Manufacturing* 11: 31–38.
- Franken M, Stramigioli S, Misra S, Secchi C and Macchelli A (2011) Bilateral telemanipulation with time delays: A two-layer approach combining passivity and transparency. *IEEE Transactions on Robotics* 27(4): 741–756.
- Gallagher W, Gao D and Ueda J (2014) Improved stability of haptic human–robot interfaces using measurement of human arm stiffness. *Advanced Robotics* 28(13): 869–882.
- Gerelli O and Bianco CGL (2009) Nonlinear variable structure filter for the online trajectory scaling. *IEEE Transactions on Industrial Electronics* 56(10): 3921–3930.
- Ginos B (2009) *Parameter Estimation for the Lognormal Distribution*. Master's Thesis, Brigham Young University.
- Grafakos S, Dimeas F and Aspragathos N (2016) Variable admittance control in phri using emg-based arm muscles co-activation. In: *Proceedings of the IEEE International Conference on Systems, Man, and Cybernetics*, pp. 001900–001905.
- Hannaford B and Ryu JH (2002) Time-domain passivity control of haptic interfaces. *IEEE Transactions on Robotics and Automation* 18(1): 1–10.
- Hubert M and Vandervieren E (2008) An adjusted boxplot for skewed distributions. *Computational Statistics and Data Analysis* 52(12): 5186–5201.
- Johnson N, Kotz S and Balakrishnan N (1995) *Continuous Univariate Distributions (Probability and Mathematical Statistics, volume 1 and 2)*. 2nd ed. New York: Wiley.

- Lamy X, Colledani F, Geffard F, Measson Y and Morel G (2009) Achieving efficient and stable comanipulation through adaptation to changes in human arm impedance. In: *Proceedings of the IEEE International Conference on Robotics and Automation*, pp. 265–271.
- Lecours A, Mayer-St-Onge B and Gosselin C (2012) Variable admittance control of a four-degree-of-freedom intelligent assist device. In: *Proceedings of the IEEE International Conference on Robotics and Automation*.
- Lee D and Huang K (2010) Passive-set-position-modulation framework for interactive robotic systems. *IEEE Transactions on Robotics* 26(2): 354–369.
- Okunev V, Nierhoff T and Hirche S (2012) Human-preference-based control design: Adaptive robot admittance control for physical human–robot interaction. In: *Proceedings of the IEEE International Conference on Robot and Human Interactive Communication*, pp. 443–448.
- Peer A and Buss M (2008) Robust stability analysis of bilateral teleoperation systems using admittance-type devices. In: *Proceedings of the SICE Annual Conference*, Tokyo, Japan.
- Podobnik J and Munić M (2007) Haptic interaction stability with respect to grasp force. *IEEE Transactions on Systems, Man, and Cybernetics, Part C (Applications and Reviews)* 37(6): 1214–1222.
- Ranatunga I, Lewis FL, Popa DO and Tousif SM (2017) Adaptive admittance control for human–robot interaction using model reference design and adaptive inverse filtering. *IEEE Transactions on Control Systems Technology* 25(1): 278–285.
- Rosenstrauch MJ and Kruger J (2017) Safe human–robot collaboration - introduction and experiment using ISO/TS 15066. In: *Proceedings of the International Conference on Control, Automation and Robotics*.
- Ryu D, Song JB, Kang S and Kim M (2008) Frequency domain stability observer and active damping control for stable haptic interaction. *IET Control Theory and Applications* 2(4): 261–268.
- Schmidtler J, Bengler K, Dimeas F and Campeau-Lecours A (2017) A Questionnaire for the Evaluation of Physical Assistive Devices (QUEAD). In: *Proceedings of the IEEE International Conference on Systems, Man and Cybernetics*, pp. 876–881.
- Secchi C, Stramigioli S and Fantuzzi C (2006) Position drift compensation in Port–Hamiltonian based telemanipulation. In: *Proceedings of the IEEE/RSJ International Conference on Intelligent Robots and Systems*, pp. 4211–4216.
- Talignani Landi C, Ferraguti F, Sabattini L, Secchi C, Bonfè M and Fantuzzi C (2017a) Variable admittance control preventing undesired oscillating behaviors in physical human–robot interaction. In: *Proceedings of the IEEE International Conference on Intelligent Robots and Systems*, Vancouver, Canada.
- Talignani Landi C, Ferraguti F, Sabattini L, Secchi C and Fantuzzi C (2017b) Admittance control parameter adaptation for physical human–robot interaction. In: *Proceedings of the IEEE International Conference on Robotics and Automation*, Singapore.
- Talignani Landi C, Ferraguti F, Secchi C and Fantuzzi C (2016) Tool compensation in walk-through programming for admittance-controlled robots. In: *Proceedings of the Annual Conference of IEEE Industrial Electronics Society*, Firenze, Italy.
- Tsumugiwa T, Yokogawa R and Hara K (2002) Variable impedance control based on estimation of human arm stiffness for human–robot cooperative calligraphic task. In: *Proceedings of the IEEE International Conference on Robotics and Automation*, Vol. 1, pp. 644–650.
- Tsumugiwa T, Yokogawa R and Yoshida K (2004) Stability analysis for impedance control of robot for human–robot cooperative task system. In: *Proceedings of the IEEE/RSJ International Conference on Intelligent Robots and Systems*, Sendai, Japan.
- Villani L and De Schutter J (2008) Force control. In: Siciliano B and Khatib O (eds.) *Springer Handbook of Robotics*. Berlin: Springer.

## Appendix. Index to multimedia extensions

Archives of IJRR multimedia extensions published prior to 2014 can be found at <http://www.ijrr.org>, after 2014 all videos are available on the IJRR YouTube channel at <http://www.youtube.com/user/ijrrmultimedia>

**Table of Multimedia Extensions**

Extension	Media type	Description
1	Video	Video of the experiments described in the paper.